Available online at www.sciencedirect.com

jmr&t Journal of Materials Research and Technology

www.jmrt.com.br

Original Article

Effects of pin diameter and number of cycles on microstructure and tensile properties of friction stir fabricated AA1050-Al_2O_3 nanocomposite

R. Darzi Bourkhani[a], A.R. Eivani[a,*], H.R. Nateghi[b], H.R. Jafarian[a]

[a] School of Metallurgy and Materials Engineering, Iran University of Science and Technology (IUST), Narmak, Tehran, Iran
[b] Department of Mechanical Engineering, Politecnico di Milano, Milano, Italy

ARTICLE INFO

Article history:
Received 14 November 2019
Accepted 21 February 2020
Available online 17 March 2020

Keywords:
Al
Al_2O_3
Nanocomposite
Additive fabrication

ABSTRACT

Nanocomposites of Al-Al_2O_3 are fabricated by means of friction stir processing (FSP). Effects of pin diameter and number of FSP cycles on tensile properties of the nanocomposites are investigated and the variations are correlated to the evolution of microstructure and distribution of nanoparticles in addition to agglomeration of Al_2O_3 nanoparticles. Investigation of agglomeration has been considered as an indirect indication for efficiency of the process for distribution of nanoparticles. The ductility of the nanocomposite is found to improve due to grain refinement during FSP. However, the ductility is likely to degrade if Al_2O_3 particles agglomerate and form coarse particles. The composite fabricated using the 6-mm pin indicates the maximum ductility which is attributed to formation of fine grain structure and efficient distribution of nanoparticles in the composite. Although, the grain structure in the composite fabricated using 8-mm pin is well refined, this sample shows significantly lower ductility with respect to the other samples. This was attributed to formation of coarse agglomerated particles. The second pass of FSP is found to slightly improve ductility and strength in composites fabricated using 4- and 6-mm pins but enforce significant improvements in the one with 8-mm pin. This is indeed because the second pass results in significant change in the distribution of nanoparticles or agglomerated particles in the latter case and negligible in the former ones. Grain structure and nanoparticle distribution and agglomeration can all affect the fracture surface of the tensile specimens of the fabricated nanocomposite to be ductile or brittle.

1. Introduction

In recent years, applications of composite materials are growing fast as they provide simultaneous improvements in hardness, strength, wear resistance and ductility [1]. In addi-

* Corresponding author.
E-mail: aeivani@iust.ac.ir (A. Eivani).
https://doi.org/10.1016/j.jmrt.2020.02.078

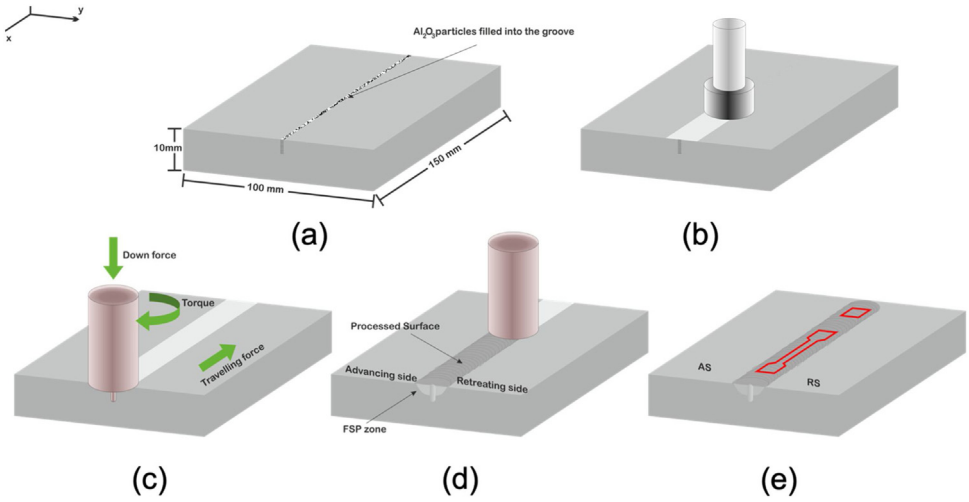

Fig. 1 – Schematic illustration of the fabrication procedure of the nanocomposite by means of FSP, (a) preparation of a groove as particle insert, (b) capping the groove after it is filled in with the nanoparticles, (c) start of FSP, (d) different regions of the microstructure of the nanocomposite and (e) the places at which the tensile test samples and microstructure specimens were extracted.

tion, special properties of the materials, such as thermal and electrical conductivity, may be subject of improvement by fabrication of composites. Metal matrix composites (MMCs) are among those composites that normally provide good ductility and fracture toughness in addition to high wear resistance and surface hardness [1]. This is indeed because the metallic matrix provides the ductility of the composite and the hardness and wear resistance would be improved by addition of hard particles which are mostly ceramics [2–4]. This behavior may be more easily facilitated with fabrication of surface composites. Surface composites demand for less production costs and complexity when compared with bulk composite production methods [5–7].

Laser melting [5], accumulative roll bonding (ARB) [8,9] and friction stir processing (FSP) [7,10] are among the production methods of surface composites. In addition, accumulative roll bonding (ARB) is a method which has been used for production of sheet metal MMCs [8,9]. Among these methods, the FSP and ARB are interesting because they provide possibility for improvement of microstructure of the metallic matrix in addition to production of composite [8,11]. Therefore, further improvement in the mechanical properties of the composite may be achieved as the microstructure is refined. FSP processing has been widely used for this purpose [3,4,6,12]. For example, composites of Al/SiC [13,14], CNT [15–17], TiC [18,19] and Al_2O_3 [20–22] have been fabricated by FSP.

FSP is a complicated thermomechanical process in which many factors, rotation and cross head speed of the pin, number of passes and tool geometry, can be effective on the final microstructure of the processed specimens [10]. The situation becomes more complicated when the process is used for production of composites. In fact, the method of addition of nanoparticles in addition to their characteristics such as composition, size and surface energy affect the final microstructure and properties of the composite [3,4,6,12]. For example, the distribution of nanoparticles in the composite can affect the evolution of microstructure by Zener pinning effect [23,24]. Therefore, although the effective parameters of FSP processing on microstructure and properties are reasonably understood and the optimum conditions are known, however, when effects of these processing parameters are combined with their mutual effects on distribution of particles in the composite, the final results of microstructure and mechanical properties may be significantly changed leading to other optimum conditions.

In recent years, additive manufacturing (AM) has achieved extensive research interest. However, due to difficulties of processing multicomponent samples, it has not acquired sufficient interest in manufacturing composites. The aim of the current investigation is to manufacture nanocomposites of Al-Al_2O_3 using an additive approach in which the reinforcing particles are added into the substrate in one or further processing steps. In addition, it is important to understand the mutual effects of variations in pin diameter and number of FSP cycles as the processing parameters on the distribution of nanoparticles in a composite of Al-Al_2O_3 fabricated by FSP. Although three pin diameters are investigated, the aim of the current investigation is not to optimize the pin diameter but to see how properties change with its variation as well as finding the correlative explanation for the variations. For this purpose, FSP is used to fabricate Al-Al_2O_3 nanocomposites with using three different pin diameters. The FSP is repeated two times. Evolution of microstructure and tensile properties are assessed and the results are inter-correlated to the distribution of nanoparticles and agglomeration of few others.

2. Experimental procedure

Nanocomposite of aluminum with alumina nanoparticles was fabricated using friction stir processing (FSP). Schematic illustration of the fabrication process is shown in Fig. 1(a). The

Table 1 – Composition of the AA1050 aluminum alloy used as matrix.

Element	Cu	Mg	Si	Fe	Mn	Zn	Ti	Al
wt%	0.03	0.03	0.25	0.3	0.05	0.06	0.04	Balance

aluminum matrix was 10 mm thick hot rolled sheet AA1050 alloy provided by IRALCO aluminum industries. Chemical composition of the alloy is shown in Table 1. The plates were annealed at 510 °C for 1 h and cooled down in the furnace prior to FSP. The sheets were cut into rectangular plates of 100 × 50 mm. A 1 mm wide and 3 mm deep groove was machined in the plates with the purpose of adding the reinforcing particles. Pre-synthesized Al_2O_3 nanoparticles with a size range of less than 100 nm were used as reinforcing particles. The nano-powder was dried for 1 h at 40 °C to remove water prior to addition to the matrix. The machined groove was filled with the nano-powder.

FSP was conducted for 1 and 2 cycles using tools with 20 mm shoulder diameter, 100 mm height and a pin with 5 mm in height and different diameters. The diameters of the pins which were made of quenched and tempered H13 tool steel were different, i.e., 4, 6 and 8 mm. The rotation and crosshead speeds were 1180 rpm and 80 mm/min, respectively. The tool was tilted for 3° and was moved down so far that the shoulder penetrated into the matrix plate for 0.3 mm.

In order to investigate microstructure and mechanical properties of the fabricated nanocomposites, samples were extracted from the top side, approximately 2 mm beneath the surface with 2 mm thickness. In other words, it can be said that the selected area of investigation fall from 2 to 4 mm below the surface of the FSP fabricated nanocomposite. A schematic illustration showing the location of the tensile test and microstructure investigation samples are shown in Fig. 1(c). Similar samples were extracted for other characterization purposes, i.e., optical microscopy (OM), SEM, tensile testing and tribology.

HUVITZ-HR3-TRF-P optical microscope was used to study the evolution of microstructure. The samples were extracted from the regions as schematically shown in Fig. 1(e). The samples were grinded and polished after cutting and etching using HBF_4 in distilled water. A Tescan-Vega3 SEM was used for scanning electron microscopy. Tensile testing was conducted on subsized specimens with 2 mm thickness, 3 mm width and 50 mm length, according to ASTM E8-04 standard. The location at which the tensile test specimens are extracted are shown in Fig. 1(e). Santam STM-20 tensile testing machine was used to conduct the tests at 0.5 mm/min.

3. Results and discussion

3.1. *Characteristics of the constituents of the nanocomposite*

The nanocomposite which was fabricated in this investigation had two constituents, i.e., AA1050 aluminum matrix and Al_2O_3 nanoparticles. Optical microstructure of the AA1050 aluminum matrix after annealing at 510 °C for 1 h has been shown in Fig. 2(a). It can be seen that a fully recrystallized microstructure has formed after annealing the initially received hot rolled plates. Presence of a combination of fine and coarse grains with an average size of 128 μm are observed. Tensile stress-strain curve of the sample after annealing and prior to FSP is shown in Fig. 2(b). Uniform elongation (eu) of 26% is observed which represents the tensile elongation of a fully annealed product of aluminum. The extracted yield strength (YS) and ultimate tensile strength (UTS) of the sample were 28 and 50 MPa, respectively. Accordingly, one may conclude that the utilized annealing treatment has been successfully applied to delete the effects of previous thermomechanical processes during production.

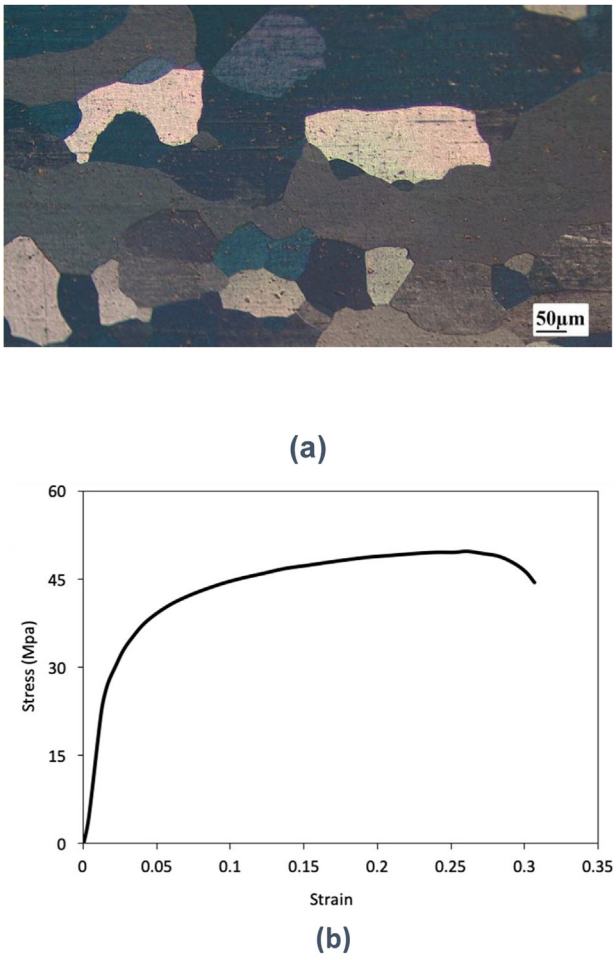

Fig. 2 – (a) Optical microstructure of the AA1050 aluminum alloy after annealing at 510 °C for 1 h, (b) tensile stress-strain curves of the initial sample.

High magnification SEM image of the Al_2O_3 nanoparticles used as reinforcing particles in fabrication of the nanocomposite are shown in Fig. 3(a). In addition, an EDS spectrum showing the result of chemical analysis of the particles are presented in Fig. 3(b). It can be seen that the size range of the utilized particles is in general within less than 100 nm. The particles are composed of Al and O and no signs of impurity are detected during EDS measurements.

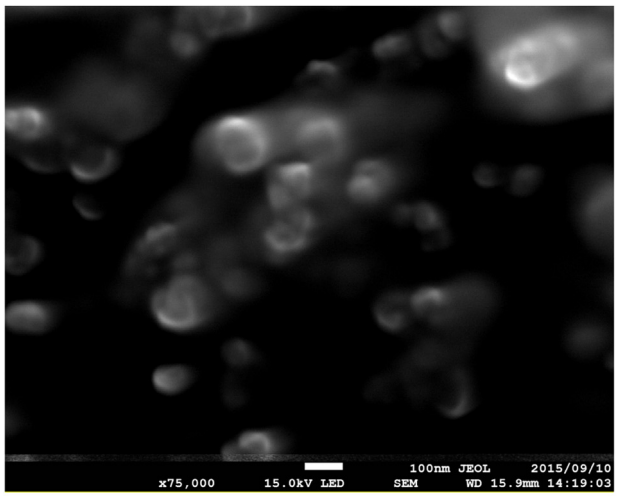

(a)

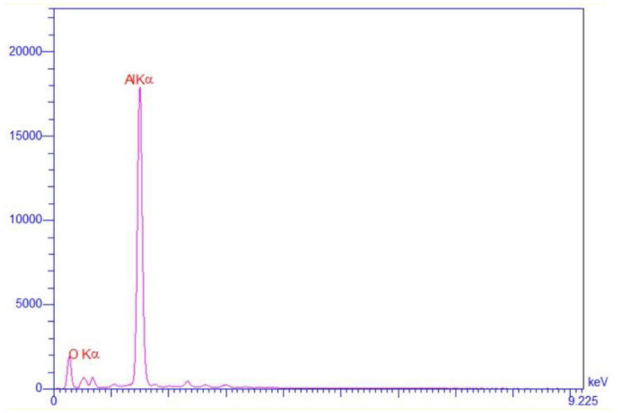

(b)

Fig. 3 – (a) SEM image showing the size and morphology of reinforcing Al_2O_3 nanoparticles and (b) EDS spectrum of the nanoparticles.

3.2. *First cycle of processing*

3.2.1. *Tensile properties*

Effects of one cycle of FSP using different pin diameters on stress-strain curves of the fabricated nanocomposites are shown in Fig. 4(a). Yield strength (YS), ultimate tensile strength (UTS) and uniform elongation (e_u) are extracted. The extracted data are presented in Fig. 4(b). In addition, the variations in tensile properties are quantified and presented in Fig. 4(c). It can be seen that in all cases the flow stress, YS and UTS of the fabricated MMCs are higher than the base metal (BM). In addition, elongation is enhanced when FSP is conducted using 4- and 6-mm pins. However, in the case of MMC produced using 8-mm pin, elongation has reduced. The maximum enhancement in strength is observed in the case of the one processed using 4-mm pin while the one processed using 6-mm pin shows an increased enhancement in strength but the maximum ductility. Ductility has reduced in the case of the sample

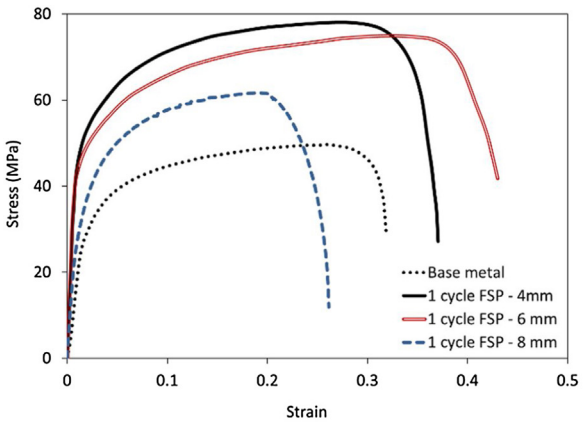

(a)

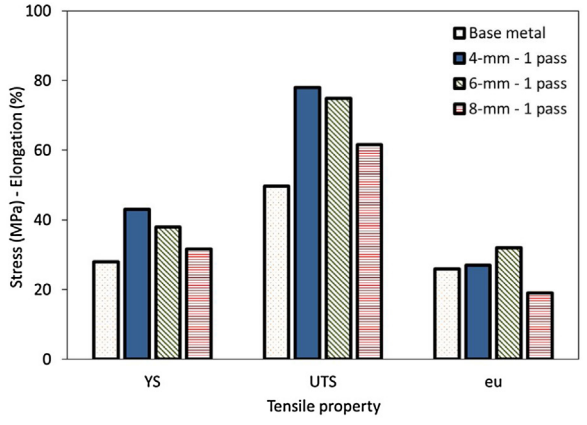

(b)

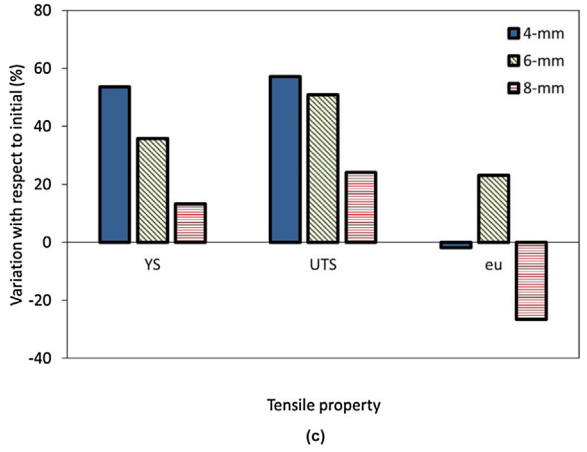

(c)

Fig. 4 – (a) Tensile stress-strain curves of the nanocomposites fabricated using 4-, 6- and 8-mm pins in comparison to that of the base metal prior to fabrication, (b) extracted values for tensile properties and (c) levels of improvement in comparison to the base metal.

processed using 8-mm pin in spite of the minimum enhancement in strength. Therefore, it can be concluded that the 8-mm pin does not provide a convenient condition for fabrication of such composites. In addition, depending on the fact that whether strength is of the outmost importance or ductility, the 4- and 6-mm pins are desirable, respectively. Considering the negligible variations in strength and the fact that ductility is a determining factor in selection and performance of fabricated structural MMCs, 6-mm may be considered the more convenient pin diameter for the purpose of fabrication of such nanocomposites.

3.2.2. *Fracture surface*

Fracture surfaces of the tensile samples extracted from fabricated nanocomposites using tools with pins of different diameters are shown in Fig. 5. It can be observed that ductile fracture by dimple rupture mechanism has occurred due to overload during tensile testing. The fracture surfaces are in overall divided into two regions, i.e., the central fibrous dimple rupture and peripheral smooth fast fracture surfaces. Representative images of these two regions are shown at higher magnifications aside each figure. These two regions are presented in all the three samples, although they showed significantly different ductility in terms of elongation to failure in Fig. 4.

The main difference is the fractional area of dimple rupture and fast fracture surfaces. Indeed, the central dimple rupture region is smallest for the sample fabricated by 8 mm pin and larger for those fabricated by 4 and 6 mm pins. With increasing deformation by necking during tensile testing, the microvoids nucleate at regions of localized strain discontinuity, e.g., second phase particles, inclusions and dispersed nanoparticles. Microvoid formation on the dispersed nanocomposites is more likely in the case of the present nanocomposites than formation on other types of strain discontinuities. If these nanoparticles are more efficiently dispersed, dimples form at higher density. However, if they are agglomerated and not efficiently dispersed, dimples form at lower number density and cause fewer dimples, leading to more significant growth of the dimples during tensile test and eventually coarser dimples and premature fracture. As indicated by red dashed line circles, many of these nanoparticles which are agglomerated and form particles in the size range of 10 μm are observed in the roots of the dimples which indicates their role in nucleation and formation of dimples. Therefore, smaller dimple rupture region is in line with the existence of extra coarse dimples which join each other fast and cause eventual fracture. This is in line with smaller elongation to failure of the nancomposite fabricated by 8 mm pin.

In addition to the fractional area of the dimple rupture regions, their size, shape and morphology are subject to change during tensile testing. It can be seen that the average dimple size is the largest for the one fabricated by 8 mm pin. Dimples are smaller for the two nanocomposites prepared by 4 and 6 mm pins with negligible difference between them. Dimple size on the fracture surface is governed by the number and distribution of microvoids. Larger dimples are formed when the nucleation cites are few and widely spaced. This leads to the fact that the microvoids grow to a large size before coalesce, resulting in large dimples. However, when numerous

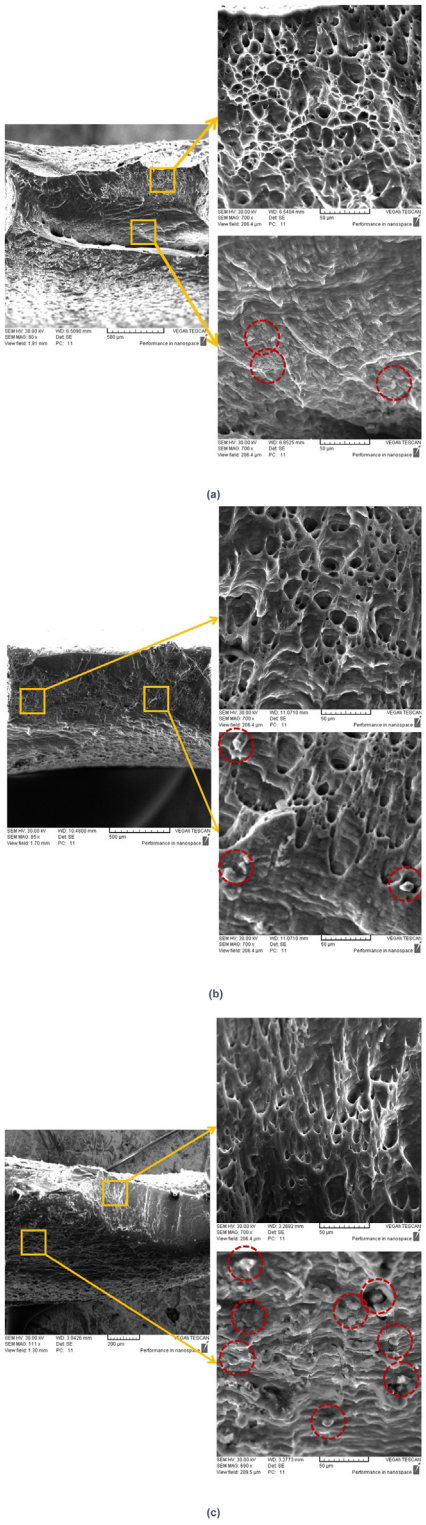

Fig. 5 – Overall fracture surface of the tensile specimens from nanocomposites fabricated by one pass of FSP using pins with (a) 4, (b) 6 and (c) 8 mm diameter.

nucleating cites are activated, before getting the opportunity to grow significantly, they join each other and lead to final fracture. Accordingly, it can be concluded that if the reinforcing nanoparticles are well distributed, i.e., in the case of 4 and 6 mm pins, they form a higher density of nucleation cites, leading to finer dimples. In contrast, when there is a large number of agglomerated nanoparticles which means less efficient distribution and more stress localization and more considerable strain discontinuity in addition to more nonuniformity in the distribution of nanoparticles result in nucleation and growth of isolated microvoids early in the loading cycle leading to less ductility and an eventual fracture surface with various dimple sizes, see Fig. 5(c). As mentioned earlier, extra coarse dimples formed by growth of microvoids can result in sufficient weakening of the tensile specimen to undergo fast fracture by tensile tearing. Open end elongated dimples are observed in Fig. 5(b) and (c) which are likely to be formed during the last steps of tensile fracture, i.e., tensile tearing by shear. Formation of the indicated fracture features in Fig. 5(c), e.g., cleavage steps, river patterns and chevron patterns are indication of occurrence of brittle fracture in the last steps of tensile testing.

3.2.3. *Distribution of nanoparticles*

SEM micrographs showing the distribution of Al_2O_3 nanoparticles in the fabricated composites using 4-mm pin are shown in Fig. 6. A relatively uniform distribution of nanoparticles in the sample indicates the efficiency of the FSP for producing MMC nanocomposites. Successful application of the method has been previously reported by other researchers [4,11]. Therefore, enhancement of strength of the alloy after FSP processing may be attributed to the formation of Al-Al_2O_3 nanocomposite.

In addition, coarse white particles are observed in the middle of this image. Investigation of these coarse particles is extremely important as the observations and be used as indirect indications for the efficiency of the FSP process and the applied parameters, i.e., rotation and crosshead speed in addition to pin diameter. Indeed, due to the fact that these particles are very small, see Fig. 3(a), an attempt on capturing an image with distribution of nanoparticles would not yield an image better than the one presented in Fig. 6. Such images, although of great importance to the investigation, but does not provide a quantitative assessment of the efficiency of the process. Therefore, indirect approach, i.e., consideration of the size and distribution of agglomerated nanoparticles, has been chosen as a more valuable approach. EDS analysis on these particles indicates that they are compounds of Al and O, most likely Al_2O_3. Considering the purity of the base metal used in this investigation, existence of such big constituent particles is not expected. Therefore, these may be attributed to the agglomeration of the Al_2O_3 nanoparticles which has been previously observed [11]. Existence of these particles can be significantly harmful to the properties of the composites as they play the specific role of crack initiation which results in eventual fracture and reduced ductility during tensile deformation. Consequently, the tensile elongation of the samples would be limited by the amount, fraction and size of these particles [25,26]. Non-uniformity in distribution of nanoparticles can also significantly affect deformation and may result in localized deformation which eventually leads to reducing duc-

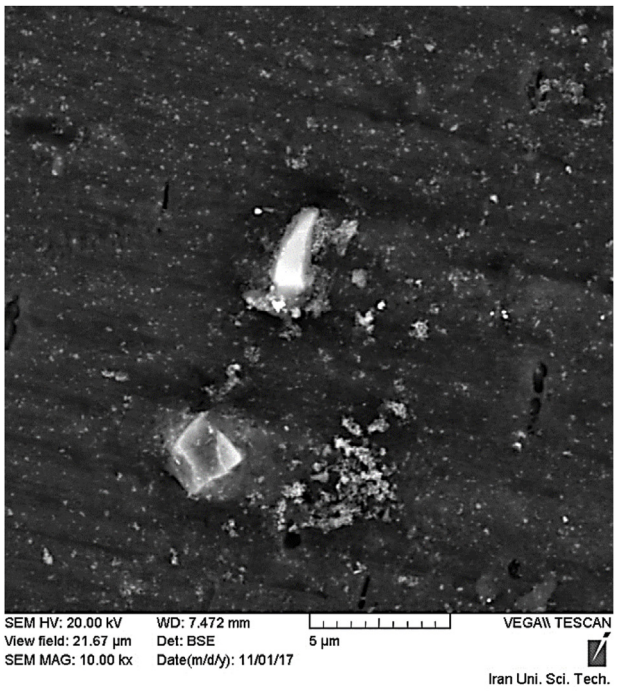

Fig. 6 – (a) High and (b) low magnification SEM images showing the distribution and agglomeration of Al_2O_3 nanoparticles in one pass FSP processed composite using 4-mm pin.

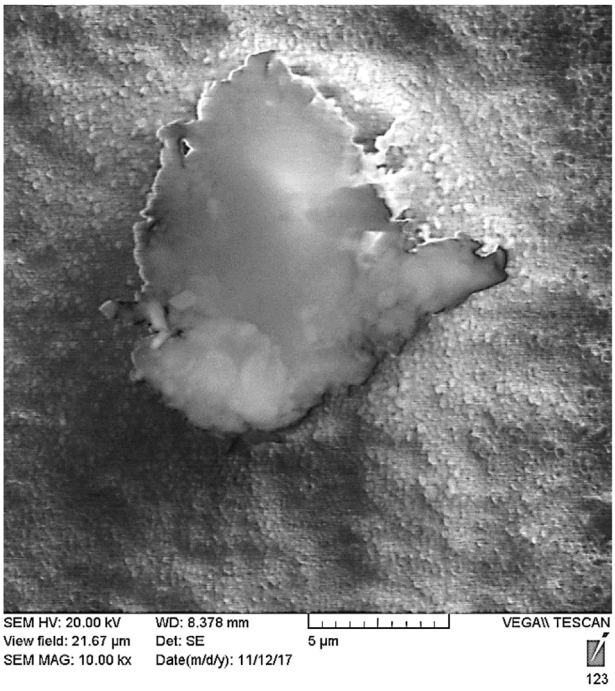

Fig. 7 – SEM image showing the distribution and agglomeration of Al_2O_3 nanoparticles in one pass FSP processed composite using 8-mm pin.

Table 2 – Quantitative information of the particles in the fabricated composites.

Sample	Average particle size (μm)	Maximum particle size (μm)
4mm-FSP-1	0.85 ± 0.1	3.50 ± 0.4
6mm-FSP-1	1.03 ± 0.1	3.14 ± 0.3
8 mm-FSP-1	1.40 ± 0.2	7.16 ± 0.7
4mm-FSP-2	0.82 ± 0.1	2.96 ± 0.3
6mm-FSP-1	0.83 ± 0.1	1.60 ± 0.2
8 mm-FSP-2	1.03 ± 0.1	6.06 ± 0.7

tility. This is indeed, in addition to agglomeration of particles which directly affects fracture. In order to have a clearer image of the extent of agglomeration, an SEM image in lower magnification is captured and shown in Fig. 6(b). Few white particles within the size range of micrometers can be observed in this image. These particles can act as the locations for initiation of cracks and reduce the ductility of the composite.

An SEM image which show a coarse agglomerated Al_2O_3 particles in the composite fabricated using the 8 mm pin is shown in Fig. 7. It can be seen that the particles are extremely coarse, of size range of larger than 5 μm. Indeed, it is clear that the size and the number density of these particles are larger than the one fabricated using the 4-mm pin. In order to be able to make solid conclusions on the effects of pin diameter on the distribution and sizes of nanoparticles, quantitative analysis was conducted using ImageJ and the results are presented in Table 2. Quantitative results show that the average size of agglomerated particles is the minimum in the 4-mm processed specimen and the maximum in 8-mm processed one. However, the 6-mm processed specimen provides the smallest value for the maximum size of the agglomerated particles. Therefore, the highest ductility of 6-mm processed specimen can be attributed to having fewer coarse particles. In addition, application of 8-mm pin has not been successful in fabrication of an MMC with optimized and efficient distribution of nanoparticles and more extended agglomeration has occurred. As these large particles may act as locations for crack initiation, one may expect a significant drop in the ductility of the nanocomposite including such big particles. This is in line with the poor ductility of this sample presented in Fig. 4.

3.2.4. *Microstructure*

Despite of the fact that all samples processed using FSP with addition of nanocomposites include coarse agglomerated particles, it can be seen in Fig. 4 that the elongations of the composites fabricated using 4- and 6-mm pins are enhanced with respect to the initial sample. It is true that these two samples are in possession of finer agglomerated particles and consequently higher ductility with respect to the 8-mm processed one, however, the enhancement in ductility of these samples comparing with the base metal with no addition of particles is un-known. Indeed, as the coarse particles can act as locations for crack initiation and result in reduced ductility, there should be another factor which plays role in determination of ductility. Microstructures of the fabricated nanocomposites in comparison with the microstructure of the BM are shown in Fig. 8. It can be seen that regardless of pin diameter, the grain structures of the samples have been significantly refined with FSP processing. Therefore, enhancement of ductility of the nanocomposites may be attributed to grain refinement. Indeed, there would a competition between the positive effects of grain refinement on improvement of ductility and consecutive negative effects of the agglomerated particles. It can be concluded that in the case of the nanocomposite fabricated by 8-mm pin, the particles are so large that the positive effects of grain refinement on ductility disappears and ductility reduces with FSP.

3.3. *Effects of second cycle of FSP*

3.3.1. *Microstructure and tensile properties*

Effects of second cycle of FSP on tensile behavior of the fabricated nanocomposites are shown in Fig. 9. Tensile characteristics of the fabricated nanocomposites, i.e., YS, UTS and e_u, were extracted from these curves and presented in Fig. 10(a). In addition, the variations in tensile properties of the two passes processed composites with respect to one pass and comparing with the base metal, are presented in Fig. 10(b) and (c), respectively. It can be seen that in the case of the composites fabricated with 4- or 6-mm pins, the strength and ductility have slightly improved with applying two cycles of FSP. Microstructures of the samples after the second pass of FSP are shown in Fig. 11. Quantitative analysis of the microstructures show that the average grain size has slightly reduced. Negligible reduction in grain size can serve as an explanation for enhancement of strength and ductility in the composites produced by 4- and 6-mm pins. However, in the case of the nanocomposite fabricated using 8-mm pin, the ductility is significantly enhanced with applying the second pass of FSP which cannot be simply explained by such small variation in

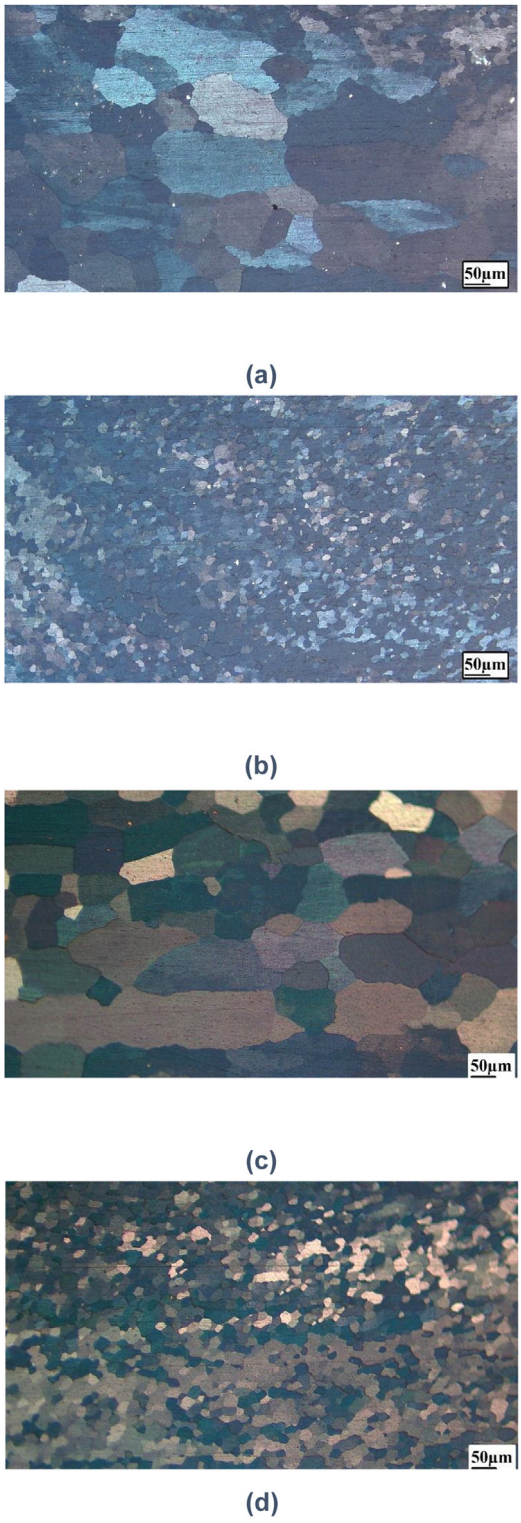

Fig. 8 – Microstructures of the (a) and (c) BM and (b) and (d) nanocomposite fabricated by FSP using (a) and (b) 4 mm and (c) and (d) 8 mm pins.

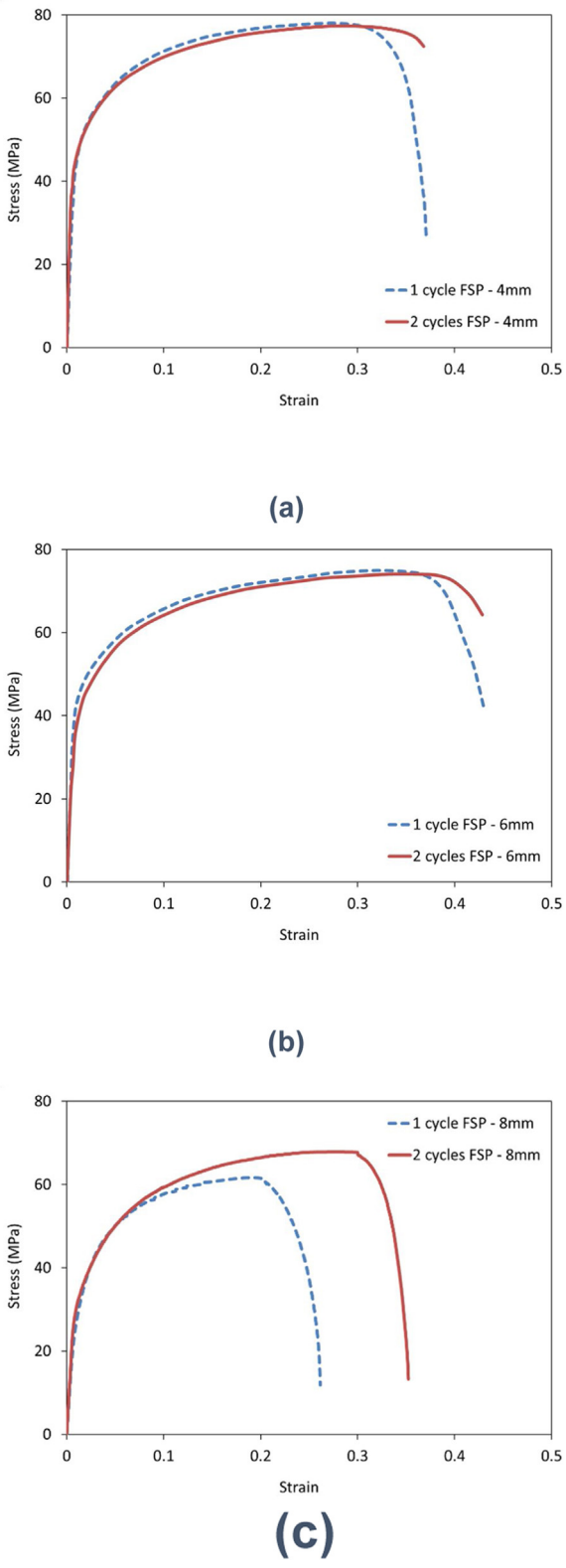

Fig. 9 – Stress-strain curves of the fabricated nanocomposites with pins of (a) 4, (b) 6 and (c) 8 mm diameter.

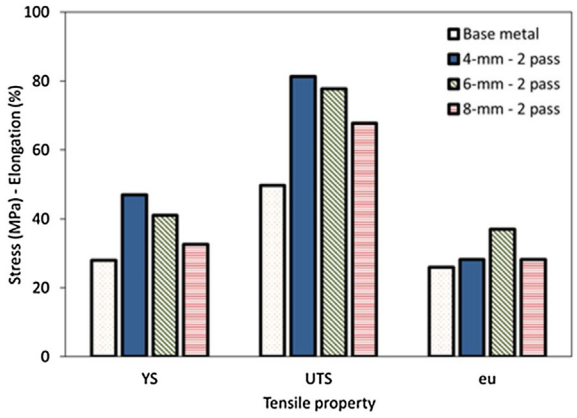

(a)

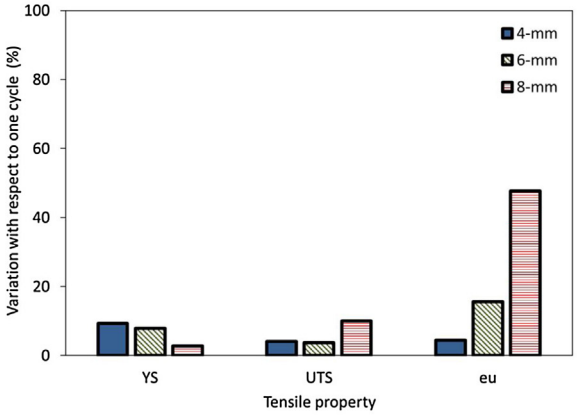

(b)

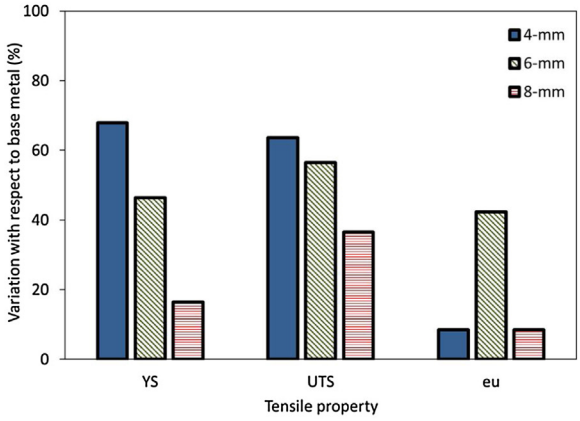

(c)

Fig. 10 – Tensile characteristics of the nanocomposites fabricated using one and two passes of FSP with pins of (a) values after the second cycle and variations with respect to (b) the one cycle fabricated samples and (c) base material.

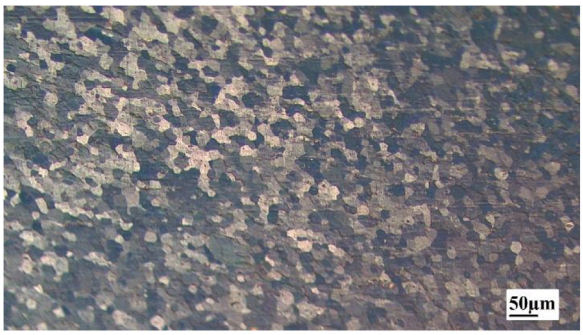

(a)

(b)

Fig. 11 – Microstructures of the samples after the second pass of FSP using pins of (a) 4 and (b) 8 mm diameter.

grain size. Therefore, variations in the distribution of Al_2O_3 nanoparticles and the significance of agglomeration should be investigated.

3.3.2. *Fracture surface*

The effect of second cycles of FSP on the fracture surface of tensile specimens of the fabricated nanocomposites are shown in Fig. 12. It can be seen that the dimple rupture region in all cases are larger than those observed after 1 cycle FSP. This is likely to be due to the fact that more efficient distribution of nanoparticles create further nucleation cites for microvoids, consequently less growth before reaching each other. Therefore, dimples are finer and shallower indicating smaller deformation of each single dimple prior to failure. As mentioned earlier, extra coarse dimples formed by growth of microvoids can result in sufficient weakening of the tensile specimen to undergo fast fracture by tearing. Therefore, more efficient distribution of nanoparticles leading to denser dimple formation can postpone fast fracture of the specimen and consequently, increase the ductility, observed in the form of increased elongation to failure in tensile test results. It can be concluded that the reason behind significant increase in the elongation to failure of the 8 mm-pin fabricated nanocomposite is the considerable achievement in efficiency of distribution of nanoparticles by applying the second cycle of FSP with respect to the sample with one cycle of FSP.

It is also interesting to note that less number of the coarse agglomerated nanoparticles are observed at the bottom of the

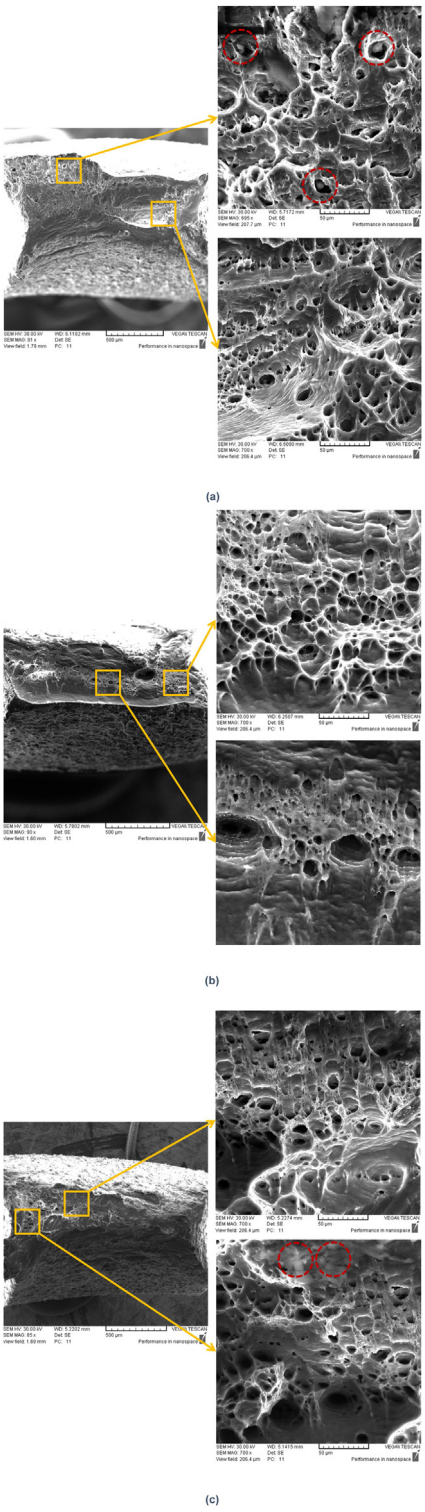

Fig. 12 – Fracture surface of the tensile specimens from nanocomposites fabricated by two passes of FSP using a pin with (a) 4, (b) 6 and (c) 8 mm diameter.

Table 3 – Variations in average and maximum particles sizes resulting from the second pass of FSP.

Pin diameter (mm)	Reduction in average particle size (%)	Reduction in maximum particle size (%)
4	3.5	15.4
6	19.4	33.1
8	26.4	41.3

dimples which is likely to be due to more efficient distribution of nanoparticles caused by the second cycle of FSP. This can even change the mechanism of fracture from ductile rupture to tearing topography surface (TTS). In TTS, the fracture appears to be the result of a microplastic tearing on submicron scale. Indeed, microvoids do not exhibit large plastic deformation to form dimples, instead form relatively smooth areas containing tear ridges, as indicated in Fig. 12(b). Such fracture topography may have been formed due to the nucleation of closely spaced microvoids, limited growth before coalescence and leading to very shallow dimples.

3.3.3. *Distribution of nanoparticles*

SEM micrographs present show second phase particles and nanoparticles in the fabricated composites using 4- and 8-mm pins are shown in Fig. 13. Comparison between the images related to the composite of 4-mm pin with those after the first pass of FSP shows negligible variations. Indeed, the distribution of agglomerated particles is slightly changed while the nanoparticle distribution is almost un-changed. However, quantification of the results as presented in Table 3, indicates that the average particle size and the size of the maximum observed particles are reduced. In order to make a solid conclusion, the reduction in particle sizes after the second pass of the FSP with respect to the first pass and presented in Table 3. This reduction in particles sizes would help with enhancement of ductility of the composite. Variations in the case of 8 mm pin are significant. Such big particles as shown in Fig. 7, are disappeared. Indeed, these particles are re-distributed in the matrix by application of the second cycle of FSP. Therefore, the enormous enhancement in ductility should be attributed to fragmentation of agglomerated particles. Despite of having the maximum ductility in the first pass of FSP, the 6-mm processed sample shows a considerable reduction in the second pass and consequently, a considerable enhancement in ductility.

4. Conclusions

In this investigation, friction stir processing (FSP) is used for fabrication of Al-Al_2O_3 nanocomposites. Three different pin diameters are used for this purpose and the effect of pin diameter on the evolution of microstructure and tensile properties are investigated. According to the results of this investigation, the following conclusions are made;

1 The strength and flow stress of the fabricated nanocomposites are higher than the base metal (BM). Provided that an efficient distribution of nanoparticles occurs in the composite, the ductility of the composite would be larger than

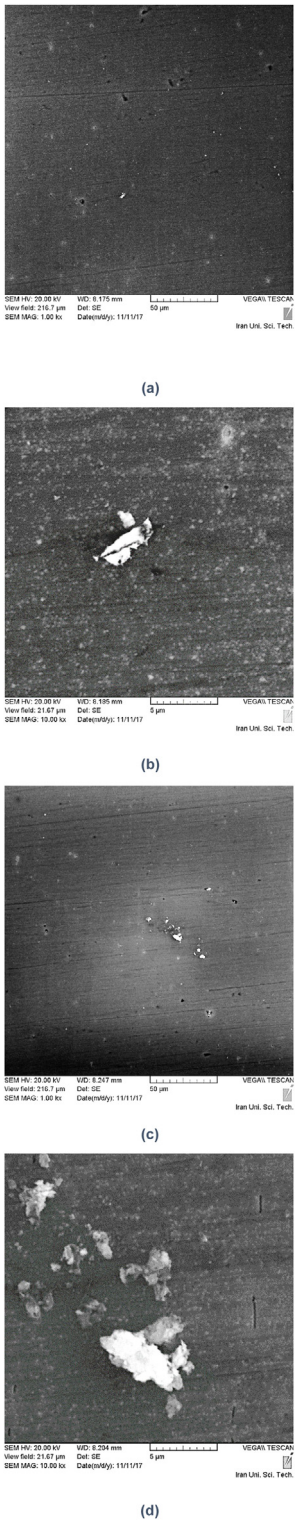

Fig. 13 – SEM micrographs showing the evolution in the distribution of (a) and (c) agglomerated particles and (b) and (d) nanoparticles in the second pass of FSP using pins of (a) and (b) 4 and (c) and (d) 8 mm.

the initial sample. This is attributed to formation of fine grain structure after FSP. For the sample which is fabricated using the 8-mm pin, extremely coarse agglomerated particles form which annihilate the positive effects of grain refinement on ductility and result in significantly reduced ductility of the composite.

2 The second cycle of FSP is found to result in more efficient distribution of Al_2O_3 nanoparticles and consequently, lead to increased ductility. However, the improvement is insignificant in the case of the samples fabricated using pins of 4- and 6-mm. This is indeed due to the fact that an efficient distribution of nanoparticles occurs in the first cycle of fabrication of these composites which are not supposed to considerable improvement with applying the second FSP cycle.

3 The improvement in ductility is thoroughly comprehensive in the case of the sample processed using 8-mm pin. This is indeed because of the fact that the first cycle of FSP using 8-mm pin cannot efficiently distribute the nanoparticles and lead to formation of extra-large agglomerated particles and reduced ductility. Re-distribution of agglomerated particles is considered as the controlling factor which results in improved ductility.

4 FSP processing using 6-mm pin results in the maximum achievements in terms of simultaneous improvement in ductility and strength. In comparison to 4 mm pin, the fracture surface of the tensile specimens indicates improved ductility by utilization of the 6-mm pin. This is attributed to considerable grain refinement, efficient distribution of the nanoparticles throughout the matrix of the composite and minimum agglomeration. Indeed, the maximum particle size is the smallest for the samples processed using the 4mm-pin.

Conflicts of interest

The authors declare no conflicts of interest.

REFERENCES

[1] Casati R, Vedani M. Metal matrix composites reinforced by nano-particles—a review. Metals 2014;4:65–83, http://dx.doi.org/10.3390/met4010065.

[2] Smagorinski ME, Tsantrizos PG, Grenier S, Cavasin A, Brzezinski T, Kim G. The properties and microstructure of Al-based composites reinforced with ceramic particles. Mater Sci Eng A 1998;244:86–90, http://dx.doi.org/10.1016/S0921-5093(97)00830-7.

[3] Shafiei-Zarghani A, Kashani-Bozorg SF, Zarei-Hanzaki A. Microstructures and mechanical properties of Al/Al2O3 surface nano-composite layer produced by friction stir processing. Mater Sci Eng A 2009;500:84–91, http://dx.doi.org/10.1016/j.msea.2008.09.064.

[4] Koli DK, Agnihotri G, Purohit R. A review on properties, behaviour and processing methods for Al- nano Al2O3 composites. Procedia Mater Sci 2014;6:567–89, http://dx.doi.org/10.1016/j.mspro.2014.07.072.

[5] Kruth J-P, Mercelis P, Vaerenbergh JV, Froyen L, Rombouts M. Binding mechanisms in selective laser sintering and

selective laser melting. Rapid Prototyp J 2005, http://dx.doi.org/10.1108/13552540510573365.
[6] Morisada Y, Fujii H, Nagaoka T, Fukusumi M. MWCNTs/AZ31 surface composites fabricated by friction stir processing. Mater Sci Eng A 2006;419:344–8, http://dx.doi.org/10.1016/j.msea.2006.01.016.
[7] Mishra RS, Ma ZY, Charit I. Friction stir processing: a novel technique for fabrication of surface composite. Mater Sci Eng A 2003;341:307–10, http://dx.doi.org/10.1016/S0921-5093(02)00199-5.
[8] Jafarian H, Habibi-Livar J, Razavi SH. Microstructure evolution and mechanical properties in ultrafine grained Al/TiC composite fabricated by accumulative roll bonding. Compos Part B Eng 2015;77:84–92, http://dx.doi.org/10.1016/j.compositesb.2015.03.009.
[9] Jamaati R, Toroghinejad MR. Manufacturing of high-strength aluminum/alumina composite by accumulative roll bonding. Mater Sci Eng A 2010;527:4146–51, http://dx.doi.org/10.1016/j.msea.2010.03.070.
[10] Ma ZY. Friction stir processing technology: a review. Metall Mater Trans A 2008;39:642–58, http://dx.doi.org/10.1007/s11661-007-9459-0.
[11] Bourkhani RD, Eivani AR, Nateghi HR. Through-thickness inhomogeneity in microstructure and tensile properties and tribological performance of friction stir processed AA1050-Al2O3 nanocomposite. Compos Part B Eng 2019;174:107061, http://dx.doi.org/10.1016/j.compositesb.2019.107061.
[12] Lee CJ, Huang JC, Hsieh PJ. Mg based nano-composites fabricated by friction stir processing. Scr Mater 2006;54:1415–20, http://dx.doi.org/10.1016/j.scriptamat.2005.11.056.
[13] Uzun H. Friction stir welding of SiC particulate reinforced AA2124 aluminium alloy matrix composite. Mater Des 2007;28:1440–6.
[14] Dolatkhah A, Golbabaei P, Givi MB, Molaiekiya F. Investigating effects of process parameters on microstructural and mechanical properties of Al5052/SiC metal matrix composite fabricated via friction stir processing. Mater Des 2012;37:458–64.
[15] Liu ZY, Xiao BL, Wang WG, Ma ZY. Singly dispersed carbon nanotube/aluminum composites fabricated by powder metallurgy combined with friction stir processing. Carbon 2012;50:1843–52.
[16] Liu Q, Ke L, Liu F, Huang C, Xing L. Microstructure and mechanical property of multi-walled carbon nanotubes reinforced aluminum matrix composites fabricated by friction stir processing. Mater Des 2013;45:343–8.
[17] Izadi H, Gerlich AP. Distribution and stability of carbon nanotubes during multi-pass friction stir processing of carbon nanotube/aluminum composites. Carbon 2012;50:4744–9.
[18] Bauri R, Yadav D, Suhas G. Effect of friction stir processing (FSP) on microstructure and properties of Al–TiC in situ composite. Mater Sci Eng A 2011;528:4732–9.
[19] Rejil CM, Dinaharan I, Vijay SJ, Murugan N. Microstructure and sliding wear behavior of AA6360/(TiC+ B4C) hybrid surface composite layer synthesized by friction stir processing on aluminum substrate. Mater Sci Eng A 2012;552:336–44.
[20] Shafiei-Zarghani A, Kashani-Bozorg SF, Zarei-Hanzaki A. Microstructures and mechanical properties of Al/Al2O3 surface nano-composite layer produced by friction stir processing. Mater Sci Eng A 2009;500:84–91, http://dx.doi.org/10.1016/j.msea.2008.09.064.
[21] Shafiei-Zarghani A, Kashani-Bozorg SF, Zarei-Hanzaki A. Wear assessment of Al/Al2O3 nano-composite surface layer produced using friction stir processing. Wear 2011;270:403–12.
[22] Koli DK, Agnihotri G, Purohit R. A review on properties, behaviour and processing methods for Al-nano Al_2O_3 composites. Procedia Mater Sci 2014;6:567–89.
[23] Shahani RA, Clyne TW. Recrystallization in fibrous and particulate metal matrix composites. Mater Sci Eng A 1991;135:281–5.
[24] Humphreys FJ, Miller WS, Djazeb MR. Microstructural development during thermomechanical processing of particulate metal-matrix composites. Mater Sci Technol 1990;6:1157–66.
[25] Lewandowski JJ, Liu C, Hunt WH Jr. Effects of matrix microstructure and particle distribution on fracture of an aluminum metal matrix composite. Mater Sci Eng A 1989;107:241–55.
[26] Brechet Y, Embury JD, Tao S, Luo L. Damage initiation in metal matrix composites. Acta Metall Mater 1991;39:1781–6.